Specificity in substrate and cofactor recognition by the N-terminal domain of the chaperone ClpX

Guillaume Thibault, Jovana Yudin, Philip Wong, Vladimir Tsitrin, Remco Sprangers, Rongmin Zhao, and Walid A. Houry

PNAS published online Nov 7, 2006;
doi:10.1073/pnas.0601505103

Specificity in substrate and cofactor recognition by the N-terminal domain of the chaperone ClpX

Guillaume Thibault, Jovana Yudin, Philip Wong*, Vladimir Tsitrin†, Remco Sprangers, Rongmin Zhao, and Walid A. Houry‡

One King's College Circle, Medical Sciences Building, Department of Biochemistry, University of Toronto, Toronto, ON, Canada M5S 1A8

Edited by Susan Gottesman, National Institutes of Health, Bethesda, MD, and approved October 3, 2006 (received for review February 23, 2006)

Clp ATPases are a unique group of ATP-dependent chaperones supporting targeted protein unfolding and degradation in concert with their respective proteases. ClpX is a representative member of these ATPases; it consists of two domains, a zinc-binding domain (ZBD) that forms dimers and a AAA+ ATP-binding domain that arranges into a hexamer. Analysis of the binding preferences of these two domains in ClpX revealed that both domains preferentially bind to hydrophobic residues but have different sequence preferences, with the AAA+ domain preferentially recognizing a wider range of specific sequences than ZBD. As part of this analysis, the binding site of the ClpX dimeric cofactor, $SspB_2$, on ZBD in ClpX was determined by NMR and mutational analysis. The SspB C terminus was found to interact with a hydrophobic patch on the surface of ZBD. The affinity of $SspB_2$ toward ZBD_2 and the geometry of the $SspB_2$–ZBD_2 complex were investigated by using the newly developed quantitative optical biosensor method of dual polarization interferometry. The data suggest a model for the interaction between $SspB_2$ and the ClpX hexamer.

NMR | SspB | zinc-binding domain

Protein degradation is an essential component of biological regulation and protein quality control in all organisms. Cylindrical proteases, such as the proteasome, form large oligomers in which the proteolytic active sites are sequestered within an internal chamber. Access to the chamber is provided through narrow axial pores that exclude entry of large polypeptides and allow entry only of small peptides of ≈30 residues in length (1). These cylindrical proteases typically form complexes with ATPases associated with various cellular activities (AAA+) chaperones that denature substrates and then translocate them into the proteolytic chamber of the protease for degradation.

ClpXP of *Escherichia coli* forms such a complex (2). ClpX is the AAA+ ATPase, and it belongs to the Clp/Hsp100 family, whereas ClpP is a cylindrical serine protease consisting of two rings with 7-fold symmetry (3). ClpX has an N-terminal domain followed by a AAA+ domain (Fig. 6*A*, which is published as supporting information on the PNAS web site). The importance of the N-terminal domain of ClpX is evident from its absolute conservation across all sequenced genomes (4). Our group demonstrated that the N-terminal domain of ClpX is a C4-type zinc-binding domain (ZBD) that forms a very stable constitutive symmetric dimer in isolation and in full-length ClpX. ZBD binds one Zn(II) per monomer (4, 5). Hydrophobic residues that form the interface between two ZBD monomers are highly conserved throughout the sequenced genomes (5). The AAA+ domain forms a hexameric ring complex in a nucleotide-dependent manner from which the ZBD protrudes (Fig. 6*B*). ClpX unfolds proteins and then feeds them into ClpP for degradation.

Two proteins that were initially recognized as ClpX substrates are the phage proteins λO and MuA. More recently, ≈50 endogenous *E. coli* ClpX substrates were identified through a proteomics approach (6). ClpXP has also been implicated in the degradation of C-terminally SsrA-tagged proteins. GFP with an SsrA sequence added to its C terminus has typically been used as a model substrate to study such tagged proteins (7). The $SspB_2$ cofactor enhances the degradation efficiency of C-terminally SsrA-tagged proteins by ClpXP (8). The SspB polypeptide can be divided into a substrate-binding domain that forms a dimer and a C-terminal unstructured domain that binds to the ZBD in ClpX (9). It has been proposed that $SspB_2$ binds to SsrA-tagged proteins forming a complex that subsequently binds to the ClpX hexamer (10). Hence, the binding of $SspB_2$, loaded with substrate, to ZBD in ClpX functions to hold the substrate in place as the AAA+ domain of ClpX pulls the substrate, starting from the recognition motif, through ClpX and into ClpP for degradation. It is established that both C-terminal tails in the SspB dimer are required to enhance the degradation of SsrA-tagged substrates by ClpXP (11). Although the ZBD in ClpX is required to bind the cofactor $SspB_2$, the ZBD is not required to bind and degrade SsrA-tagged proteins (4).

Here we address the question of how the ZBD of ClpX recognizes substrates/cofactors. To this end, we initially used peptide array analysis to determine the general binding preferences of ZBD_2 and compared those to the binding preferences of the AAA+ domain. Subsequently, we carried out NMR, mutational, and thermodynamic interaction studies to further characterize and map the binding site of $SspB_2$ on ZBD_2. The implications of our findings on $SspB_2$–$ClpX_6$ complex formation are discussed.

Results

ZBD and AAA+ Domains of ClpX Preferentially Bind to Hydrophobic Residues. To determine the roles of the ZBD and AAA+ (ClpXΔZBD) domains of ClpX in substrate and cofactor recognition, peptide array analysis was carried out to identify residues that are preferentially bound by these two domains of the chaperone (Fig. 7, which is published as supporting information on the PNAS web site). Purified ZBD_2 or AAA+ domains were incubated with peptide arrays containing a total of 3,717 C-terminally attached peptides whose sequences were derived from 26 different proteins, some of which are known ClpX substrates (see *Materials and Methods*). The ZBD is dimeric under all conditions used (4, 5). Because substrates entering into ClpX hexamer will bind to the interior chamber of the AAA+ ring, and because the oligomerization of the AAA+ ring requires the presence of nucleotides (12), peptide array

Author contributions: G.T. and W.A.H. designed research; G.T., J.Y., and R.Z. performed research; G.T. and R.S. contributed new reagents/analytic tools; G.T., J.Y., P.W., V.T., and W.A.H. analyzed data; and G.T. and W.A.H. wrote the paper.

The authors declare no conflict of interest.

This article is a PNAS direct submission.

Abbreviations: AAA+, ATPases associated with various cellular activities; ZBD, zinc-binding domain; ITC, isothermal titration calorimetry.

*Present address: Institute for Bioinformatics, Gesellschaft für Strahlung und Umweltforschung, National Research Center for Environment and Health, Ingolstadter Landstrasse 1, D-85764 Neuherberg, Germany.

†Present address: Harmonic Enterprise Systems, 512-50 Ruddington Drive, Toronto, ON, Canada M2K 2J8.

‡To whom correspondence should be addressed. E-mail: walid.houry@utoronto.ca.

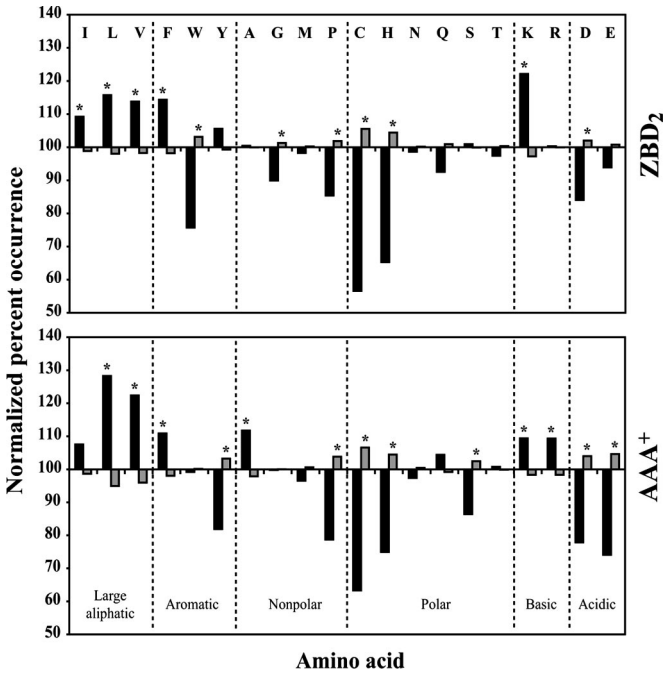

Fig. 1. Analysis of ZBD- and AAA$^+$-binding preferences using peptide arrays. Shown are the ZBD_2 and AAA$^+$ residue-binding preferences. The normalized percent occurrence for each amino acid was determined for both the binder (black bars) and nonbinder (gray bars) groups. Asterisk indicates that the difference between the occurrence of an amino acid in the binder group and on the array is significant at the 95% confidence level using the *z* test (22).

Table 1. Peptide sequence patterns preferentially bound by ZBD_2 and AAA$^+$

ZBD_2		AAA$^+$	
Rank	Pattern	Rank	Pattern
1	[ST]xEx[ILMV]	1	[ST]Lxx[ILMV]
2	[ST]x[DE]xL	2	Rx[ILMV][ILMV]
3	**V[AG]xx[ILMV]**	3	[ILMV][ILMV][AG][AG]
4	S[ILMV]x[AG]	4	[ILMV]x[ILMV][ILMV][ILMV]
5	ALxx[ILMV]	5	[ILMV]xx[ST]L
6	[ILMV]I[QN]	6	[ILMV][ILMV][ILMV]x[AG]
7	**[AG]I[ILMV]**	7	[ILMV]xx[ILMV][ILMV][AG]
8	[FY]x[ILMV]xG	8	[ILMV]I[QN]
9	[AG][DE]xV	**9**	**V[AG]xx[ILMV]**
10	[KR][AG]xxL	10	T[ILMV]xxL
11	**[ILMV]xL[ILMV]x[AG]**	11	[ST][ILMV]L
12	[ILMV]x[ILMV][ILMV]xx[AG]	12	[ILMV]xAG
13	[ILMV][ILMV]x[ILMV]x[KR]	13	[ILMV]x[QN]L
14	[KR]x[ILMV][ILMV]x[ILMV]	14	[ILMV]xL[ILMV][ILMV]
15	[ST]xExL	15	VxL[ILMV]
		16	[AG]x[ILMV]xI
		17	LLxx[AG]
		18	[ILMV]x[ILMV][ILMV]xA
		19	**[ILMV]xL[ILMV]x[AG]**
		20	**[AG]I[ILMV]**

Residues in brackets indicate that any of the listed amino acids can be present at that position. x represents any amino acid. Patterns in bold are present in both ZBD_2 and AAA$^+$. Patterns are ranked according to F_B (see *Materials and Methods*).

analysis of the AAA$^+$ domain was carried out in the absence of nucleotides to expose the putative polypeptide-binding sites that will be involved in substrate translocation and possibly unfolding. The binding of AAA$^+$ to the peptide arrays in the presence of nucleotides was also carried out but was found to be significantly reduced (Fig. 8, which is published as supporting information on the PNAS web site); consequently, the proportion of binders was statistically insignificant, reflecting the fact that the hexamerized AAA$^+$ ring can recognize only specific sequence tags such as the SsrA tag. Hence no further analysis of the data for AAA$^+$ in the presence of nucleotides could be carried out.

Fig. 7 shows an example of the binding preferences of ZBD_2 and AAA$^+$ (in the absence of nucleotides) to arrays generated by using peptides derived from λO and MuA as detected by Western blot analysis. In general, ZBD_2 and AAA$^+$ bound different peptide sequences. For example, ZBD_2 bound strongly to peptides derived from residues Gln^{49}-Met^{67} of λO, whereas AAA$^+$ preferentially bound to peptides derived from residues Ile^{7}-Ser^{41}, Pro^{215}-Leu^{241}, and Lys^{283}-Leu^{299} of λO (Fig. 7). Because ZBD_2 binds λO and is required for λO degradation by ClpXP (4), these results suggest that the region Gln^{49}-Met^{67} of λO is essential for the recognition of λO by ClpX (see below). ZBD_2 and AAA$^+$ also recognize different MuA peptide sequences. MuA is 663 aa long. Interestingly, the C terminus of MuA, which was proposed to be the ClpX-recognition motif (13), was only weakly bound by ZBD_2, and only residues Glu^{645}-Lys^{661} were bound by the AAA$^+$ domain (Fig. 7).

In analyzing the peptide array data, peptides were classified as binders of ZBD_2 or AAA$^+$ if their normalized percent intensity was ≥75% (see *Materials and Methods*); otherwise, they were classified as nonbinders. Separation of the peptides on the arrays into binder and nonbinder groups allowed for comparison of these groups with respect to amino acid occurrence. As can be seen in Fig. 1, both ZBD_2 and AAA$^+$ preferentially bound to sequences enriched in hydrophobic residues as well as in the positively charged lysine. Negatively charged residues were typically disfavored.

ZBD_2 and AAA$^+$ Domains of ClpX Preferentially Bind to Distinct Sequence Patterns. To determine whether the ClpX domains have distinct sequence-binding preferences, and because a large data set has been obtained, binder and nonbinder peptide sequences were submitted to Teiresias (14) to search for short consensus sequences that may be responsible for ZBD_2 and AAA$^+$ binding. The Teiresias output included sequence patterns that varied in length but were generally 3–6 aa long. Patterns were analyzed as described in *Materials and Methods* to rank the consensus sequences that occurred more frequently in binders than in nonbinders (Table 1).

The utility of this approach is demonstrated by the identification of several consensus sequences previously implicated as possible ClpX-recognition sequences. For example, the strongest binding of ZBD_2 to the λO array occurs in the region Q^{49}FKVLLAILRKTYGWNKPM^{67} (Fig. 7*A*), and the patterns responsible for the binding may be [AG]I[ILMV] and [KR]x[ILMV][ILMV]x[ILMV] (ranked 7 and 14 in Table 1), corresponding to the λO region of A^{55}IL^{57} and K^{51}VLLAI^{56}, respectively. As another example, it is known that $SspB_2$ specifically binds ZBD in ClpX (4, 11). The binding is mediated by the last 10 residues in SspB (G^{156}GRPALRVVK^{165}) (9, 15), which contain the ZBD_2 consensus sequence ALxx[ILMV] (ranked 5 in Table 1). Other such consensus sequences from this analysis can be found for the putative substrates identified by Flynn *et al.* (6).

Patterns common to both ZBD_2 and AAA$^+$ binders are shown in bold in Table 1. In general, it is not surprising that there are such common patterns indicating an equal role of both domains in binding these patterns. It should be noted that more patterns were found for AAA$^+$ binders than for ZBD binders (Table 1). This might indicate that ZBD_2 exercises more specificity in substrate recognition, whereas the AAA$^+$ domain more pro-

BIOCHEMISTRY

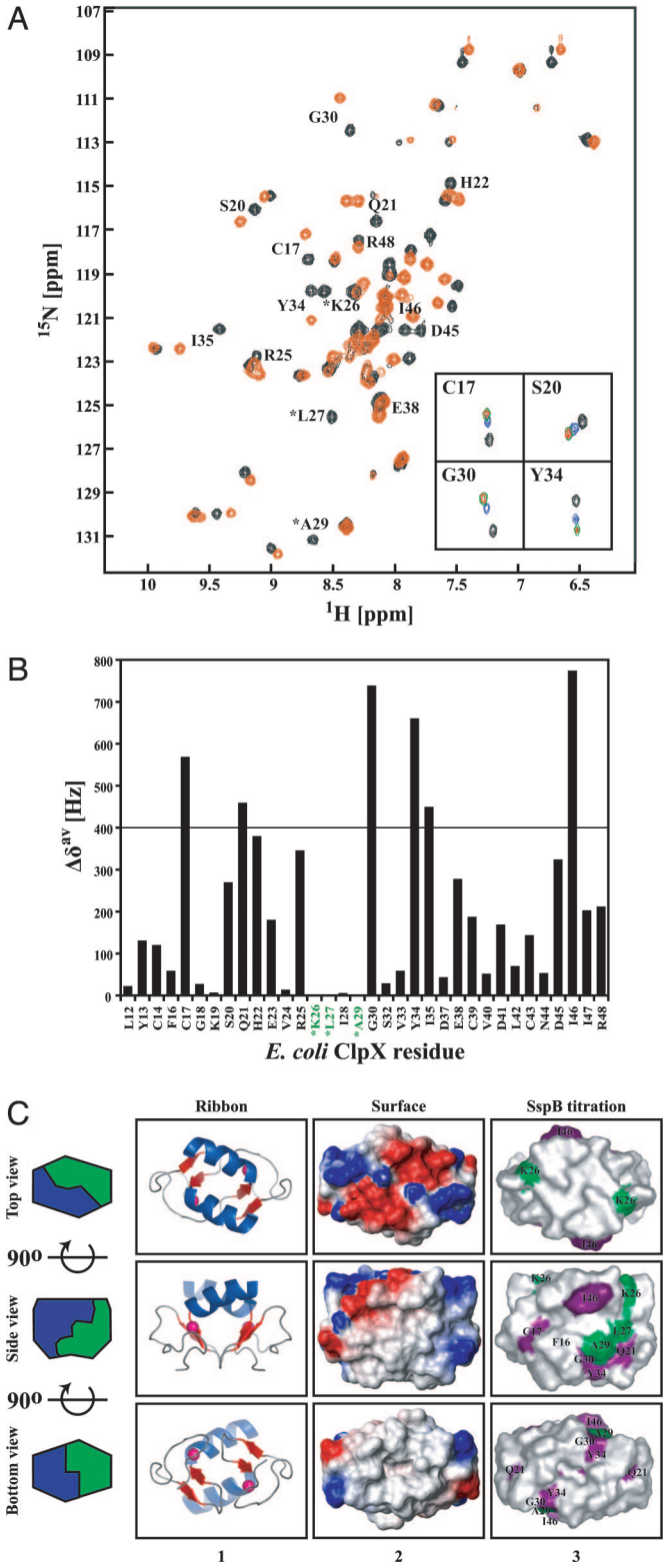

Fig. 2. Binding of SspB$^{154–165}$ to ZBD$_2$ as monitored by NMR. (*A*) A heteronuclear sequential quantum correlation spectrum of 0.25 mM ^{15}N-labeled ZBD$_2$ in the absence (black) or presence of 5 mM of SspB$^{154–165}$ (red). *, chemical shifts that disappear upon addition of peptide. *Insets* show the NH chemical shift changes of four residues in ZBD$_2$ in the presence of 0 (black), 0.5 mM (blue), 2.5 mM (green), and 5 mM (red) of SspB$^{154–165}$. (*B*) Shown are the chemical shift changes $\Delta\delta^{av} = [(\Delta\delta_{1H})^2 + (\Delta\delta_{15N})^2]^{1/2}$ in the presence of 5 mM SspB$^{154–165}$. *, residues whose chemical shifts disappeared upon addition of 5 mM SspB$^{154–165}$. (*C*) Ribbon and surface representation of ZBD dimer (Protein Data Bank ID code 1OVX) (5). *Middle* and *Bottom* are rotated 90° along the horizontal axis with respect to *Top* and *Middle*, respectively. In column 1, helices are colored blue, strands are red, and Zn(II) atoms are shown as pink spheres. In column 2, the electrostatic potential surface of ZBD$_2$ is shown with negatively charged, positively charged, and hydrophobic surfaces in red, blue, and gray, respectively. In column 3, residues for which $\Delta\delta^{av} > 400$ Hz and whose chemical shifts disappeared in the SspB$^{154–165}$ titration experiments are colored purple and green, respectively. All structures were drawn by using PyMOL (http://pymol.sourceforge.net).

miscuously binds and releases unfolded proteins as they translocate through ClpX and into ClpP.

To verify some of the results of the peptide array analysis, the following experiments were carried out. Initially, the ClpXP-mediated degradation of λO was carried in the presence of 50 times excess of the peptides λO$^{49–63}$, MuA$^{653–663}$, or SspB$^{154–165}$ (Fig. 9*A*, which is published as supporting information on the PNAS web site). According to the peptide array analysis, ZBD$_2$ bound to peptides corresponding to λO$^{49–63}$ but not to those corresponding to MuA$^{653–663}$ (Fig. 7*A*). Consistent with these results, excess of λO$^{49–63}$ peptide slowed down the ClpXP-mediated degradation of λO, whereas MuA$^{653–663}$ did not affect the rate of degradation. In addition, the C terminus of SspB, SspB$^{154–165}$ peptide, significantly slowed down λO degradation (Fig. 9*A*), suggesting that λO and SspB have similar or adjacent binding sites on ZBD in ClpX.

In another set of experiments, the peptides IYYITGESLKAVE (IYY) and DVGVLVISARKGE (DVG) were added at the N terminus of a sequence consisting of 6xHis tag followed by a tobacco etch virus recognition sequence and then GFP to form the constructs IYY-GFP and DVG-GFP, respectively. In the peptide array experiments, IYY and DVG peptides were preferentially bound by ZBD$_2$ and AAA$^+$, respectively. Consistent with those experiments, ELISA analysis confirmed that ZBD$_2$ preferentially bound IYY-GFP, whereas AAA$^+$ preferentially bound DVG-GFP (Fig. 9*B*). However, it should be noted that neither IYY-GFP nor DVG-GFP were unfolded or degraded by ClpXP (data not shown), indicating that, whereas some sequences are required for recognition by ClpX, other additional sequences might be required for unfolding and degradation.

SspB C Terminus Binds a Hydrophobic Patch on the Surface of ZBD$_2$. The peptide array analysis revealed that ZBD in ClpX might recognize a limited set of specific sequence patterns. To understand how ZBD$_2$ recognizes such sequence patterns, we endeavored to map the binding site for SspB$_2$ cofactor on ZBD$_2$. To this end, a series of ^{1}H, ^{15}N heteronuclear sequential quantum correlation spectra were recorded of a uniformly ^{15}N-labeled ZBD$_2$ in the presence of increasing concentrations of SspB$^{154–165}$ (Fig. 2*A*) or SspB$_2$ (data not shown). SspB$^{154–165}$ consists mostly of hydrophobic residues (P^{154}RGGRPALRVVK^{165}). The NH chemical shift assignments that we determined (5) were used. Upon addition of SspB$^{154–165}$, the chemical shifts of several residues systematically moved as the peptide concentration was increased (Fig. 2*A*), and saturation was typically reached at peptide to ZBD$_2$ concentration ratio between 2.5 and 5 (Fig. 2*A Inset*).

The NH groups of residues Cys^{17}, Gln^{21}, Gly^{30}, Tyr^{34}, Ile^{35}, and Ile^{46} in ZBD$_2$ (0.25 mM) shifted by >400 Hz ($\Delta\delta^{av}$; see *Materials and Methods*) in the presence of 2.5 mM of SspB$^{154–165}$ (Fig. 2*B*). Because the maximum shift observed was ≈800 Hz (Fig. 2*B*), chemical shifts more than half the maximum, i.e., >400 Hz, were arbitrarily considered to be significant. The chemical shifts of three ZBD residues (Lys^{26}, Leu^{27}, and Ala^{29}) disappeared upon addition of SspB peptide (marked by an asterisk in Fig. 2 *A* and *B*). The same phenomenon was observed upon addition of SspB$_2$

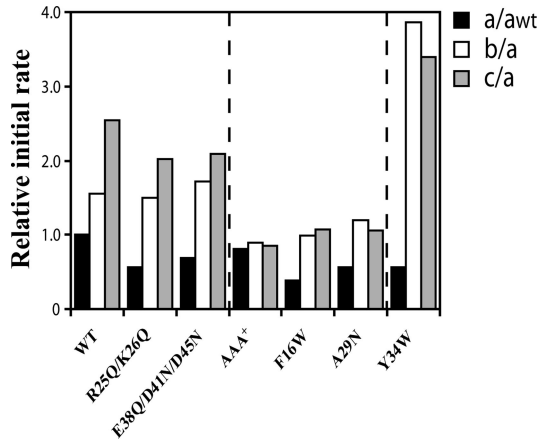

Fig. 3. Mutational analysis to determine the $SspB_2$-binding site on ZBD in ClpX. Relative initial rates of the ClpP-dependent degradation of GFP-SsrA (3.9 μM monomer concentration) mediated by ClpX or different ClpX mutants (each at 1 μM monomer concentration) in the presence of ClpP (1.2 μM monomer concentration) are shown in the presence of 0 (a), 0.025 μM (b), and 0.165 μM (c) of $SspB_2$. The initial rates a were normalized to a_{wt} (black bars), whereas the initial rates b (white bars) and c (gray bars) were normalized to the a of the respective mutant. Initial rates were determined from the first 200 seconds of the curves shown in Fig. 10.

(data not shown). Thr^1-Leu^{11}, Ser^{15}, Pro^{31}, Cys^{36}, and Glu^{49}-Arg^{60} are not observed in the ZBD_2 spectra.

ZBD_2 forms a box-shaped structure with four main surfaces. The highly charged surface of ZBD_2 is shown in Fig. 2*C Upper* (top view), two identical hydrophobic surfaces exist on both sides of the ZBD_2 box (Fig. 2*C*, side view), and a fourth hydrophobic surface is present on the bottom (Fig. 2*C*, bottom view). Residues Cys^{17}, Gln^{21}, Leu^{27}, Ala^{29}, Gly^{30}, Tyr^{34}, and Ile^{46} are part of the ZBD_2 side hydrophobic surfaces, whereas residue Lys^{26} contributes to the side hydrophobic surfaces through its long hydrophobic side chain (Cβ-ζ). Ile^{35} is part of the ZBD_2 dimer interface and is not solvent-exposed. The results strongly indicate that the side hydrophobic surfaces of ZBD_2 are the primary $SspB_2$ binding sites in ClpX; hence, there are two potential $SspB_2$-binding sites per ZBD dimer that can interact with the tails of $SspB_2$.

To further map the hydrophobic binding sites for $SspB_2$ on ZBD_2, systematic mutagenesis of the ZBD in ClpX was carried out. The degradation of GFP-SsrA was performed at 37°C in the presence of ClpP, ClpX mutants and different concentrations of $SspB_2$ and was monitored by fluorescence (Fig. 3 and Fig. 10, which is published as supporting information on the PNAS web site). As expected, $SspB_2$ does not enhance the ClpP-dependent degradation of GFP-SsrA if ClpX lacking ZBD (AAA^+) is used, because ZBD is the binding site for $SspB_2$ (4, 11). Several ClpX variants were generated with mutations in ZBD to identify mutants that behaved like AAA^+ in the degradation assays. Only mutations of the hydrophobic surfaces of ZBD in ClpX (F16W and A29N) abolished the effect of $SspB_2$, whereas replacing the positively or negatively charged residues on the charged surface of ZBD in ClpX with neutral residues (R25Q/K26Q and E39Q/D41N/D45N) did not prevent the $SspB_2$-mediated enhancement of GFP-SsrA degradation (Figs. 3 and 10). Interestingly, under the conditions used for Fig. 3, the enhancing effect of $SspB_2$ was stronger for ClpX(Y34W) as compared with ClpX WT (see also Fig. 10). Y34W is part of the hydrophobic surface of ZBD_2 (Fig. 2*C*). All mutations shown in ZBD of ClpX do not significantly affect the secondary structure content, stability, or dimerization state of isolated ZBD_2 compared with WT domain as judged by CD measurements, thermal denaturation, and size-exclusion chromatography (Fig. 11 *A–C*, which is published as supporting information on the PNAS web site). The mutation of other residues in ZBD that were identified by NMR as possible binding sites for the SspB C terminus (Fig. 2*B*) generally resulted in poorly behaved or misfolded ClpX.

The results from the mutational analysis (Fig. 3) correlate well with those from the NMR analysis (Fig. 2). The NH chemical shift for Ala^{29} disappeared upon addition of 2.5 mM SspB peptide or 125 μM $SspB_2$ full length, and for Tyr^{34}, $\Delta\delta^{av}$ was >400 Hz (Fig. 2*B* and data not shown). The NH chemical shift of Phe^{16} did not significantly change upon addition of SspB peptide or $SspB_2$ protein, which is probably because this residue is part of the dimer interface (5); however, Phe^{16} is next to Cys^{17}, which did show a $\Delta\delta^{av}$ >400 Hz in Fig. 2*B*. Hence, the NMR and mutagenesis analyses strongly suggest that residues Phe^{16}, Ala^{29}, and Tyr^{34} in ZBD of ClpX are part of or close to the $SspB_2$-binding site, and that the binding mainly occurs through the C termini of the SspB dimer.

Measuring the Binding Affinity and Geometry of the Interaction of $SspB_2$ to ZBD_2. To further support the conclusions made above, isothermal titration calorimetry (ITC) experiments were carried out at 20°C to determine the binding constant of $SspB^{154–165}$ peptide to the different ZBD_2 mutants. ZBD_2 WT bound $SspB^{154–165}$ with a K_d of 34.13 ± 5.94 μM and n = 0.97 ± 0.07 (Fig. 12 *A* and *B*, which is published as supporting information on the PNAS web site), suggesting that only one site on the hydrophobic surfaces of ZBD_2 can be saturated by the peptide. This could indicate that the binding of $SspB^{154–165}$ to one surface prevents interactions with the second surface as a result of some slight but critical conformational changes. Other interpretations are also possible. The binding of $SspB^{154–165}$ to ZBD_2(Y34W) gave a K_d of 30.49 ± 4.09 μM and n = 3.08 ± 0.04 (Fig. 12 *C* and *D*), suggesting that the mutation of Y34 to Trp allowed for the binding of the peptide to more than one site on the hydrophobic surfaces of ZBD_2(Y34W). Finally, as expected, ZBD_2(F16W) and ZBD_2(A29N) did not show any significant binding to $SspB^{154–165}$ (K_d > 200 μM; data not shown). Hence, these results, combined with the NMR and mutational analyses, strongly suggest that residues F16 and A29 are required to preserve the $SspB_2$-binding site on ZBD_2.

A further understanding of the mode of interaction of $SspB_2$ and $SspB^{154–165}$ to ZBD_2 was gained by using an AnaLight Bio200 (Farfield Scientific, Crewe, U.K.) instrument that uses a dual polarization interferometry detection method (16, 17). The instrument gives absolute measurements of thickness and density of crosslinked and bound biological molecules on films, with resolution levels of subpicogram per mm^2 and subAngstrom, respectively. ZBD_2 was crosslinked to the sensor chip by using Bis(Sulfosuccinimidyl)suberate (BS^3). Because, BS^3 reacts with primary amines, ZBD_2 is probably preferentially crosslinked with its charged surface facing the sensor chip. The thickness of ZBD_2 reached 1.93 ± 0.13 nm on the sensor chip (data not shown), close to the expected dimensions of ZBD_2. After the establishment of a stable buffer baseline, protein or peptide was injected over the immobilized ZBD_2. The thickness and density of the protein/peptide interacting with ZBD_2 on the sensor chip were then measured; hence, the mass change on the surface of the sensor chip as a function of injected sample concentration was obtained (Fig. 13 *A* and *B*, which is published as supporting information on the PNAS web site).

The binding profile for $SspB^{154–165}$ peptide was best fit to a single binding event with a K_d of 23.1 μM (Fig. 4 *A* and *C*), close to the value obtained from ITC measurements described above. On the other hand, the changes in density and thickness as a function of $SspB_2$ concentration (Fig. 13*B*), indicated there are (at least) two different binding events taking place between $SspB_2$ and ZBD_2. Fitting the mass change data to a model of two

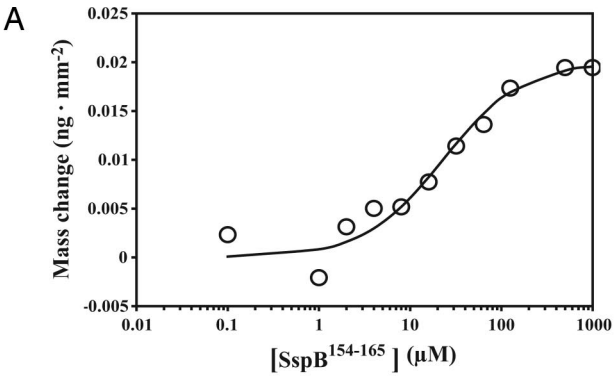

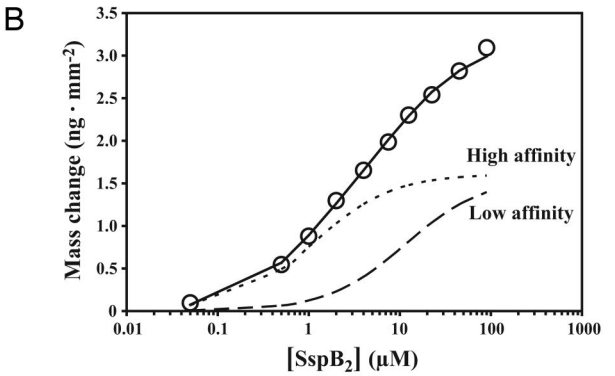

C

	$SspB^{154-165}$	$SspB_2$	
		High Affinity	Low Affinity
K_d (μM)	23.1 (4.5)	0.85 (0.11)	11.0 (2.7)
k_a ($s^{-1} M^{-1}$)	2890 (600)	1940 (124)	540 (152)
k_d (s^{-1})	0.066 (0.001)	0.0016 (0.0003)	0.006 (0.001)

Fig. 4. Determination of the binding affinity of $SspB_2$ and $SspB^{154-165}$ to ZBD_2 using dual polarization interferometry. (*A*) Open circles represent the experimental binding data of $SspB^{154-165}$ to ZBD_2, whereas the solid line represents the theoretical fit to the data assuming a single binding event. (*B*) Open circles represent the experimental data for the binding of $SspB_2$ to ZBD_2, whereas the solid line represents the theoretical fit to the data assuming two independent binding events. Curves drawn with short- and long-dashed lines represent the theoretical binding curves assuming a single binding event with K_d values given in *C* corresponding to the high- and low-affinity interactions, respectively. (*C*) Binding parameters of $SspB^{154-165}$ or $SspB_2$ to ZBD_2 obtained from the fits to the experimental data. Values in parentheses are standard deviations.

independent binding events gave a very good fit to the experimental points (Fig. 4*B*). The strong association reaction had a K_d of 0.85 μM ($SspB_2$ to ZBD_2) with a final thickness of 3.3 nm at saturation (Figs. 4*B* and 13*C*). The thickness obtained agrees with the expected dimension of a layer of SspB dimers, placed on their sides, on top of the ZBD dimers (Fig. 13*C Upper*) (5, 16, 18). The weak association reaction had a K_d of 11.0 μM ($SspB_2$ to ZBD_2) and a final thickness of 7.6 nm (Figs. 4*B* and 13*C*). The data suggest that the SspB dimer in this case is oriented vertically upon binding to ZBD_2 (Fig. 13*C*). Also, at saturation, the stoichiometry of the interaction between $SspB_2$ and ZBD_2 was found to be 1:1. It was previously reported that the binding affinity of $SspB^{154-165}$ to ClpX hexamer, $SspB^{154-165}$ to ZBD dimer, and SspB dimer to ClpX hexamer has a K_d of 22.8, 20.0, and 1.3 μM, respectively (10, 11, 15), which are close to the values obtained in our analysis (Fig. 4*C*).

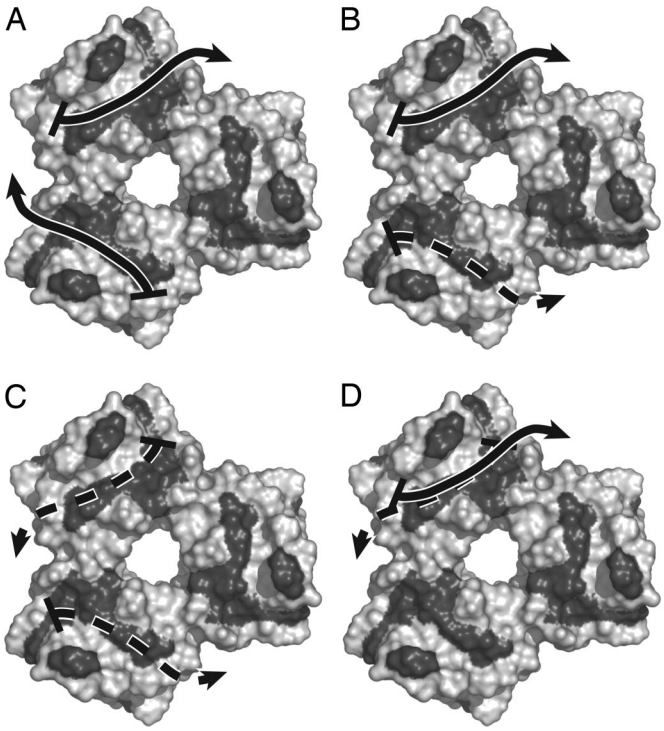

Fig. 5. Binding mode of $SspB_2$ to ZBD trimer of dimers. (*A–D*) Shown are the different possible modes of binding between two C-terminal tails of $SspB_2$ and the ZBD trimer of dimers shown in surface representation. ZBD residues implicated in interacting with SspB C terminus by NMR and mutagenesis are in a darker color. The AAA^+ ring of ClpX is assumed to be below the ZBD trimer of dimers. Arrowheads represent the N termini of the tails of $SspB_2$ and point toward the rest of $SspB_2$ body, whereas the slashes represent the C termini of the tails. Tails in dashes and in solid colors are below and above the plane of the ZBD oligomer, respectively. The three ZBD dimers might be in a more open and less planar configuration than shown.

Using this technique, it is possible to estimate the area occupied by molecules on the surface of the chip. For the high-affinity interaction, $SspB_2$ occupies an area corresponding to twice that occupied by a single ZBD_2 (Fig. 13*D*). On the other hand, for the low affinity interaction, $SspB_2$ occupies an area corresponding to a single ZBD_2 (Fig. 13*D*). We propose that the strong binding interaction is due to the association of the SspB dimer to two ZBD dimers by using both C termini of $SspB_2$, whereas the weak association interaction is due to the association of $SspB_2$ to one ZBD_2 through only one C terminus.

Discussion

Rigorous analysis of the binding of ZBD and AAA^+ domains of ClpX to a large peptide library allowed us to identify novel binding preferences for these two ClpX domains. Although ZBD and AAA^+ domains favor binding to hydrophobic residues, these domains preferentially recognize different amino acid sequences. This suggests that the ZBD and AAA^+ domains bind to different classes of polypeptides and, hence, "filter" the interaction between ClpX and its putative substrates.

The binding of $SspB_2$ to ZBD_2 occurs mainly through the interaction of the C termini of $SspB_2$ to hydrophobic patches present on the surface of ZBD_2, as determined by NMR and mutagenesis analyses (Figs. 2 and 3). The interaction is significantly enhanced by the binding of two C-terminal tails of $SspB_2$ to ZBD_2 (Fig. 4*C*). Interestingly, residue Leu^{161} at the C terminus of SspB is highly conserved and is essential for the

enhancement of the degradation of SsrA-tagged proteins by ClpXP (15). Therefore, it would be reasonable to propose that Leu^{161} of SspB is one of the C-terminal residues that directly interact with the hydrophobic patches on ZBD_2 surface.

In principle, three SspB dimers can bind to one ClpX hexamer. However, it has been experimentally determined that only one $SspB_2$ binds to a ClpX hexamer at a given time (19). We had proposed earlier that the ZBD domains in ClpX hexamer might come together to form a trimer of dimers at one stage during the chaperone functional cycle (5). Fig. 5 shows the four possible modes by which two tails of $SspB_2$ might interact with the ZBD trimer of dimers. In Fig. 5, it is assumed that the ClpX AAA^+ ring is below the ZBD_2s. Based on our binding analysis (Figs. 4, 12, and 13) and on published literature (10, 11, 15), the binding mode of Fig. 5*D* in which the two tails of $SspB_2$ interact with the same ZBD_2 is unlikely to occur, especially that an SspB tail can bind to only one site on ZBD_2 according to ITC measurements (Fig. 12). In Fig. 5 *A* and *C*, the two tails of $SspB_2$ do not interact "symmetrically" with the ZBD surface and would have to be differently kinked; this is not the case for the binding mode of Fig. 5*B*. Furthermore, in Fig. 5*C*, both tails are underneath the ZBD oligomer, between the AAA^+ ring and the ZBD_2s. We consider the modes of binding in Fig. 5 *A* and *C* to be possibly disfavored. Hence, the binding mode of Fig. 5*B* might be most likely. This mode of binding would also be in agreement with our recently published data suggesting a nucleotide-dependent block movement of the ZBD_2 toward the AAA^+ ring in ClpX (20).

In the model of Fig. 5*B*, one tail binds to the top of one ZBD_2, whereas the other tail binds to the bottom of the second ZBD_2. The third ZBD_2 can be prevented from interacting with other cofactors or substrates by the folded domain of the bound $SspB_2$. The possible movements of the ZBD_2 can then drive the bound $SspB_2$ closer to the AAA^+ ring to deliver the SsrA-tagged substrate, whereas the tails of $SspB_2$ reposition the other two ZBD_2s away from the entry pore. This model implies that the enhancing activity of $SspB_2$ is due in part to its ability to direct the movement of ZBD_2s and to regulate the delivery of tagged substrates in addition to increasing the local concentration of those substrates near ClpX.

Materials and Methods

Protein Purification and Peptide Synthesis. Proteins were expressed, purified, and manipulated as described (4). Peptides were purchased from Dalton Chemical Laboratories (Toronto, ON, Canada). CD measurements of 15 μM ZBD_2 WT and mutants were carried out in buffer A (25 mM Tris·HCl, pH 8/150 mM NaCl/1 mM DTT) by using Jasco (Easton, MD) J-810. Degradation assays were typically carried out in buffer B (25 mM Hepes, pH 7.5/5 mM $MgCl_2$/5 mM KCl/0.03% Tween-20/10% glycerol), as described (4).

Peptide Array Experiments. Peptide arrays were prepared by using an AutoSpot ASP 222 spot synthesizer (intavis AG) according to a standard spot synthesis protocol. Each peptide was 13 aa long, with a frame shift of 2 aa along the protein sequence, for a total of 3,717 peptides tested. Three independent peptide array incubation experiments were analyzed by using a procedure similar to that of Rüdiger *et al.* (21). Further details are given in *Supporting Text*, which is published as supporting information on the PNAS web site.

NMR Spectroscopy. Uniformly ^{15}N-labeled ZBD_2 was prepared by growing the *E. coli* strain BL21 gold in minimal media containing $^{15}NH_4Cl$. The NMR sample concentration was typically 0.25 mM of ZBD_2 in buffer C (20 mM sodium phosphate, pH 7.6/150 mM NaCl/10% D_2O). NMR spectra were recorded at 20°C on a 500 MHz Varian Spectrometer. ^1H, ^{15}N heteronuclear single quantum correlation experiments were carried out in the absence or presence of $SspB_2$ full length or $SspB^{154–165}$ peptide. Changes in the chemical shifts of ZBD_2 NH groups ($\Delta\delta^{av}$) were derived from $[(\Delta\delta_{1H})^2 + (\Delta\delta_{15N})^2]^{1/2}$, where $\Delta\delta$ is the chemical shift change expressed in Hz.

Measuring Binding Affinities and Geometries. ITC experiments were performed at 20°C. Twenty-nine 10-μl injections of 1.1 or 2 mM $SspB^{154–165}$ were added to 1.4 ml of 70 μM ZBD_2 or ZBD_2 mutants. Peptide and proteins were resuspended in buffer D (50 mM potassium phosphate, pH 8/75 mM NaCl/1 mM DTT). The thermograms were fit to a one-site model by using Origin 7 software (OriginLab, Northampton, MA). ITC experiments were performed by using a Microcal (Amherst, MA) VP-ITC and were repeated three times. Other binding experiments were performed by using an AnaLight Bio200 dual waveguide interferometer instrument from Farfield (16). Experiments were performed in buffer D at a flow rate of 0.05 ml/min. ZBD_2 (0.5 mg/ml) was crosslinked to both channels of the sensor chip by incubating with [Bis(sulfosuccinimidyl) suberate] (BS^3) (Pierce, Rockford, IL). Free BS^3 was blocked by using 10 mg/ml glucosamine. After the establishment of a stable buffer baseline, $SspB^{154–165}$ or $SspB_2$ was injected into one channel, whereas the second channel was used as a reference.

We thank Dr. Monika Niggermann for synthesizing some of the peptide arrays. We also thank Dr. Jimin Wang (Department of Molecular Biophysics and Biochemistry, Yale University, New Haven, CT) for helpful discussions. G.T. holds a Natural Sciences and Engineering Research Council (NSERC) PGSD2 Fellowship. J.Y. was supported by an NSERC Undergraduate Student Research Award. R.S. acknowledges financial support from a European Molecular Biology Organization postdoctoral fellowship. W.A.H. is Canadian Institutes of Health Research New Investigator. This research was supported in part by a grant from the Canadian Institutes of Health Research (to W.A.H.).

1. Thompson MW, Maurizi MR (1994) *J Biol Chem* 269:18201–18208.
2. Schirmer EC, Glover JR, Singer MA, Lindquist S (1996) *Trends Biochem Sci* 21:289–296.
3. Wang J, Hartling JA, Flanagan JM (1997) *Cell* 91:447–456.
4. Wojtyra UA, Thibault G, Tuite A, Houry WA (2003) *J Biol Chem* 278:48981–48990.
5. Donaldson LW, Wojtyra U, Houry WA (2003) *J Biol Chem* 278:48991–48996.
6. Flynn JM, Neher SB, Kim YI, Sauer RT, Baker TA (2003) *Mol Cell* 11:671–683.
7. Weber-Ban EU, Reid BG, Miranker AD, Horwich AL (1999) *Nature* 401:90–93.
8. Levchenko I, Seidel M, Sauer RT, Baker TA (2000) *Science* 289:2354–2356.
9. Dougan DA, Weber-Ban E, Bukau B (2003) *Mol Cell* 12:373–380.
10. Bolon DN, Grant RA, Baker TA, Sauer RT (2004) *Mol Cell* 16:343–350.
11. Bolon DN, Wah DA, Hersch GL, Baker TA, Sauer RT (2004) *Mol Cell* 13:443–449.
12. Grimaud R, Kessel M, Beuron F, Steven AC, Maurizi MR (1998) *J Biol Chem* 273:12476–12481.
13. Levchenko I, Yamauchi M, Baker TA (1997) *Genes Dev* 11:1561–1572.
14. Rigoutsos I, Floratos A (1998) *Bioinformatics* 14:55–67.
15. Wah DA, Levchenko I, Rieckhof GE, Bolon DN, Baker TA, Sauer RT (2003) *Mol Cell* 12:355–363.
16. Cross GH, Reeves AA, Brand S, Popplewell JF, Peel LL, Swann MJ, Freeman NJ (2003) *Biosens Bioelectron* 19:383–390.
17. Swann MJ, Peel LL, Carrington S, Freeman NJ (2004) *Anal Biochem* 329:190–198.
18. Song HK, Eck MJ (2003) *Mol Cell* 12:75–86.
19. Wah DA, Levchenko I, Baker TA, Sauer RT (2002) *Chem Biol* 9:1237–1245.
20. Thibault G, Tsitrin Y, Davidson T, Gribun A, Houry WA (2006) *EMBO J* 25:3367–3376.
21. Rüdiger S, Germeroth L, Schneider-Mergener J, Bukau B (1997) *EMBO J* 16:1501–1507.
22. Moore DS, McCabe GP (1996) *Introduction to the Practice of Statistics* (Freeman, New York).

Supporting Materials and Methods

Peptide Array Analysis. Peptides were derived from λO (Swiss-Prot # P03688), MuA (Swiss-Prot # P07636), SspB (Swiss-Prot # P0AFZ3), RepA (Swiss-Prot # P06019), ClpX (Swiss-Prot # P0A6H1), casein (Swiss-Prot # P02662), MetK (Swiss-Prot # P0A817), Dps (Swiss-Prot # P0ABT2), MDH (Swiss-Prot # P61889), LexA (Swiss-Prot # P0A7C2), MiaA (Swiss-Prot # P16384), Hsp82 (Swiss-Prot # P02829), hemagglutinin precursor (Swiss-Prot # P03438), alpha-1-antitrypsin precursor (Swiss-Prot # P01009), H-2 class I histocompatibility antigen D-B alpha chain precursor (Swiss-Prot # P01899), CD74 antigen (Swiss-Prot # P04233), spike glycoprotein precursor (Swiss-Prot # P03522), Cd3e (Swiss-Prot # P22646), Porcine citrate synthase (Swiss-Prot # P00889), PI3-kinase p85-β subunit (Swiss-Prot # O08908), UmuD (Swiss-Prot # P0AG11), σ^S (Swiss-Prot # P13445), Phd (Swiss-Prot # Q06253), λW (Swiss-Prot # P68660), eRF2 (Swiss-Prot # P05453), and acid phosphatase precursor (Swiss-Prot # P08091) sequences.

10 μg/mL of purified ZBD_2 or AAA^+ were incubated in buffer E (25 mM TrisHCl, pH 7.5, 150 mM NaCl, 0.1% Tween, 0.1% BSA, and 0.002% thimerosal) with peptide arrays previously blocked with 2% BSA in buffer E for 1 hour. The bound protein was transferred to a nitrocellulose membrane using a Hoefer TE Series semi-dry blotter (Amersham Biosciences), at 0.75 mA/cm^2 for 30 minutes using buffer F (25 mM TrisHCl, pH 8.3, 192 mM glycine, 0.1% SDS, and 20% methanol). ZBD_2 and AAA^+ were detected using rabbit polyclonal α-ClpX antibodies, and then visualized on film using Protein LA-Peroxidase (Sigma) and ECL substrate (Amersham Biosciences). Three independent peptide array incubation experiments were analyzed.

After scanning the film, spot volumes or intensities were measured using ImageQuant 5.0 (Molecular Dynamics) software. All of the spot volumes were then averaged and normalized.

Peptides that had spot intensities greater than 75% were considered binders, otherwise they were classified as non-binders. The number of each type of amino acid was counted in the binder and non-binder sequences and the percent occurrence of each amino acid in each group (binders and non-binders) and the normalized percent occurrences were calculated, as follows:

% occurrence in binders=(no. of aa 'x' in binders)/(total no. of aa in binders) x 100 (1)

Normalized % occurrence in binders=(%occurrence of aa 'x' in binders)/(%occurrence of aa 'x' on array) x 100 (2)

The z-test for comparing two proportions was used to determine if the percent occurrences of the specific amino acids in the binder or non-binder groups differed from their respective occurrences on the array at the 95% significance level.

The software Teiresias was used to search for recurring sequence patterns in the binder and non-binder peptide groups. For each sequence pattern, the frequencies of the pattern in the binder (F_B) and non-binder (F_{NB}) groups were determined by dividing the number of peptides in each group that contain the pattern by the total number of peptides in that group. The ratio R ($R = F_B/F_{NB}$) was calculated. Patterns that pass the z-test at 99.9% confidence level and that fulfill the criteria $F_B \geq 0.045$ and $R \geq 4.0$ were selected. The most general form of a sequence pattern is shown (Table 1). For example, a pattern will be reported as having [ILMV] for an amino acid instead of the version that specifically shows I, L, M, or V if both the general and specific forms of the pattern satisfy one of the three criteria listed above. The Teiresias and statistical analyses were implemented in a program developed in-house termed Sequence Array Analyzer.

ELISA assay. The wells of a 96-well plate were coated with DEA-GFP, DVG-GFP, IYY-GFP, or GFP-SsrA (100 μL, 100 μg/mL) in 20 mM Na_2CO_3, pH 9 for 1 h at 37°C. The wells were then washed with buffer I (25 mM TrisHCl, pH 7.5, 150 mM NaCl, and 0.1% Tween-20) and

incubated with 200 μL of 5% milk protein in buffer I for an additional hour at 37°C. The wells were then washed with buffer J (25 mM Hepes, pH 7.5, 150 mM KCl, 25 mM NaCl, 10 mM $MgCl_2$, 2.5% glycerol, 0.1 mM EDTA, and 0.1% Tween-20) plus 1 mM DTT and incubated with 25 μM of ZBD_2 or 1 μM AAA^+ for 1 h (total volume 100 μL). This step and all subsequent steps were performed at room temperature. Wells were washed with buffer J (200 μL, 3 times), incubated with 100 μL of a 1:3000 dilution of anti-ClpX serum for 1 h, washed, and then HRP-conjugated Protein A (1:10 000 dilution, 100 μL) in buffer J was added to the wells and incubated for 1 h. The wells were washed and 100 μL of 3,3′,5,5′-tetramethylbenzidine (TMB) liquid substrate (Sigma T0440) was added. The reaction was allowed to proceed for 30 minutes and the absorbance was measured at 650 nm using a SPECTRAmax 340PC plate reader (Molecular Devices).

Legends for Supporting Figures

Supporting Fig. 6. Structural model of the ClpXP Complex. (*A*) Shown are the domain boundaries of ZBD and AAA^+ in ClpX. (*B*) A model of the ClpXP complex. The structures shown are based on the solved structure of *E. coli* ClpP (1, 2), a model for the hexamer of the AAA^+ domain of *E. coli* ClpX based on the solved monomeric AAA^+ domain of *H. pylori* ClpX (3) and the hexameric *E. coli* HslU structure (4), and on our proposed trimer-of-dimers model for the ZBD of *E. coli* ClpX (5). Note that ClpX oligomers can bind to both ends of the ClpP cylinder. Structures were drawn using PyMOL (http://pymol.sourceforge.net).

Supporting Fig. 7. Binding of ZBD_2 and AAA^+ to the arrays of λO and MuA. (*A*) Purified

ZBD_2 or (*B*) AAA^+ in the absence of nucleotides were incubated with peptide arrays containing a total of 3717 13-mer peptides spanning the sequences of 26 proteins, with a frame shift of two amino acids. The arrays for λO and MuA are shown as examples. Labels to the left give the residue number of the N-terminal amino acid of the first peptide of each row, while labels to the right give the number of the last peptide in each row.

Supporting Fig. 8. Effect of ATP on the binding of AAA^+ to the peptide array. Purified AAA^+ was incubated with peptide arrays in the absence (top panel) or presence (bottom panel) of 5 mM ATP. The array of H-2 class I histocompatibility antigen D-B alpha chain precursor [H-2D(B)] is shown as an example. Labels to the left give the residue number of the N-terminal amino acid of the first peptide of each row, while labels to the right give the number of the last peptide in each row.

Supporting Fig. 9. Peptide-ClpX interaction. (*A*) The ClpP-dependent degradation of λO (3.9 μM monomer) mediated by ClpX (1 μM monomer) and ClpP (1.2 μM monomer) was monitored by SDS-PAGE in the absence of peptide (top lane), in the presence of 50 μM λO^{49-63} (second lane), 50 μM $MuA^{653-663}$ (third lane), or 50 μM $SspB^{154-165}$ (bottom lane) peptides. Aliquots were removed from the degradation mixture at the indicated time points. The chaperone was the last component added to the reaction mixture. (*B*) ELISA assays for the binding of 25 μM ZBD_2 or 1 μM AAA^+ (monomer concentration), respectively, to 100 μg/mL of N-terminally tagged GFP or GFP-SsrA. Data points are the average of two experiments and normalized to GFP-SsrA absorbance. DVG-GFP and IYY-GFP correspond to His-tagged GFP with the peptides DVGVLVISARKGE (DVG) and IYYITGESLKAVE (IYY), respectively, introduced at the N-

terminus. Based on Table 1, the DVG peptide contains patterns ranked 3 and 7 preferentially bound by ZBD_2 and patterns ranked 4, 6, 9, 12, 16, and 18 preferentially bound by AAA^+. The IYY peptide contains patterns ranked 1, 2, 4, 8, and 15 preferentially bound by ZBD_2 and the pattern ranked 1 preferentially bound by AAA^+.

Supporting Fig. 10. Mutational analysis to determine the $SspB_2$ binding site on ZBD in ClpX. The ClpP-dependent degradation of GFP-SsrA (3.9 μM monomer) mediated by ClpX or different ClpX mutants (each at 1 μM monomer) and ClpP (1.2 μM monomer) are shown in the presence of 0 (a), 0.025 μM (b), and 0.165 μM (c) of $SspB_2$.

Supporting Fig. 11. Stability of different ZBD_2 mutants. (*A*) CD spectra at 10°C of ZBD_2 WT and different mutants (30 μM). (*B*) Thermal denaturation curves monitored by CD at 220 nm. (*C*) The oligomeric states of the ZBD_2 mutants were analyzed by size exclusion chromatography on a Superdex 200 HR 10/30 column. Molecular mass standards, in kDa, are shown along the top. 'VV' refers to void volume. Due to the column resolution and the structure of wildtype ZBD_2, the protein elutes near the 29 kDa marker even though the molecular mass of the dimer is about 14 kDa.

Supporting Fig. 12. Determination of the binding affinity of $SspB^{154-165}$ to ZBD_2 WT and ZBD_2(Y34W) using ITC. Shown are raw ITC (*A* and *C*) and integrated heat data (*B* and *D*) of addition of $SspB^{154-165}$ to ZBD_2. Titrations were done at 20°C. Solid lines in (*B*) and (*D*) represent the fit to a model of a single type of n identical and independent binding sites. The n and K_d resulting from the fits are given.

Supporting Fig. 13. Raw data and model of the binding affinity of $SspB_2$ and $SspB^{154-165}$ to ZBD_2 using DPI. Shown are raw sensor data of addition of free $SspB^{154-165}$ (*A*) or free $SspB_2$ (*B*) to immobilized ZBD_2. T, D, and M refer to thickness, density, and mass, respectively. Different additions of $SspB^{154-165}$ or $SspB_2$ are indicated with dashed lines. The concentrations of injected $SspB^{154-165}$ or $SspB_2$ are shown on the top x-axis. (*C*) Shown are examples of the binding mode of $SspB_2$ to ZBD_2 drawn to scale. ZBD_2 on the sensor chip is drawn in light grey with the charged surface facing the chip. $SspB_2$ is shown as 2 triangles with the C-terminal tails binding to ZBD_2. Numbers on the left represent the thickness resulting from $SspB_2$ binding at saturation. Thickness measurements have an estimated error of 5 – 10%. Other modes of binding cannot be excluded. (*D*) The areas occupied by immobilized ZBD_2 and by bound $SspB_2$ in the low and high affinity interactions are given.

References

1. Wang, J., Hartling, J. A. & Flanagan, J. M. (1997) *Cell* **91,** 447-456.
2. Gribun, A., Kimber, M. S., Ching, R., Sprangers, R., Fiebig, K. M. & Houry, W. A. (2005) *J Biol Chem* **280,** 16185-16196.
3. Kim, D. Y. & Kim, K. K. (2003) *J Biol Chem* **278,** 50664-50670.
4. Bochtler, M., Hartmann, C., Song, H. K., Bourenkov, G. P., Bartunik, H. D. & Huber, R. (2000) *Nature* **403,** 800-805.
5. Donaldson, L. W., Wojtyra, U. & Houry, W. A. (2003) *J Biol Chem* **278,** 48991-48996.

Supporting Figure 6

A

B

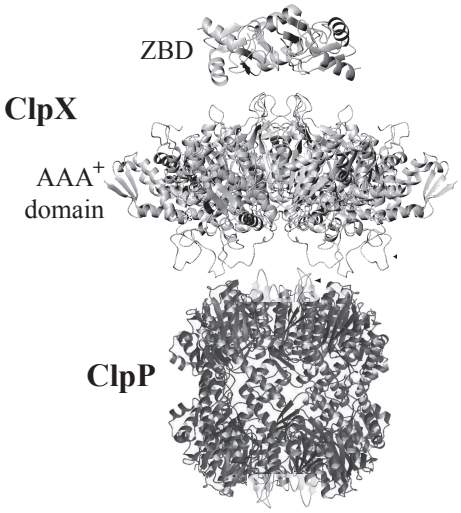

Supporting Figure 7

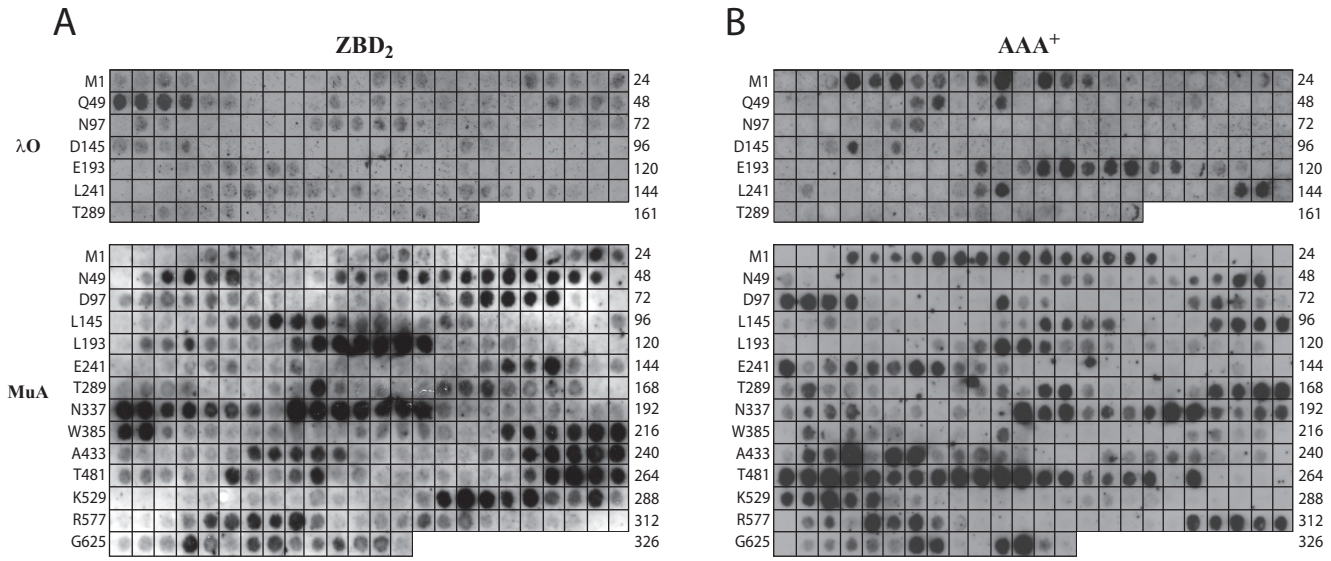

Supporting Figure 8

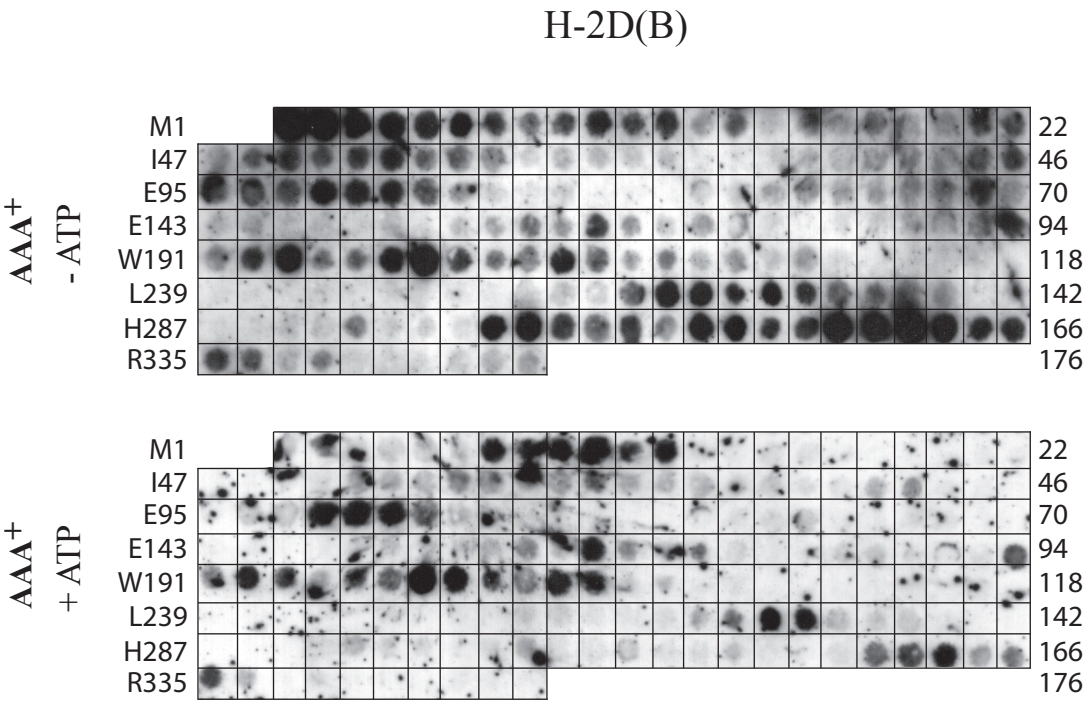

Supporting Figure 9

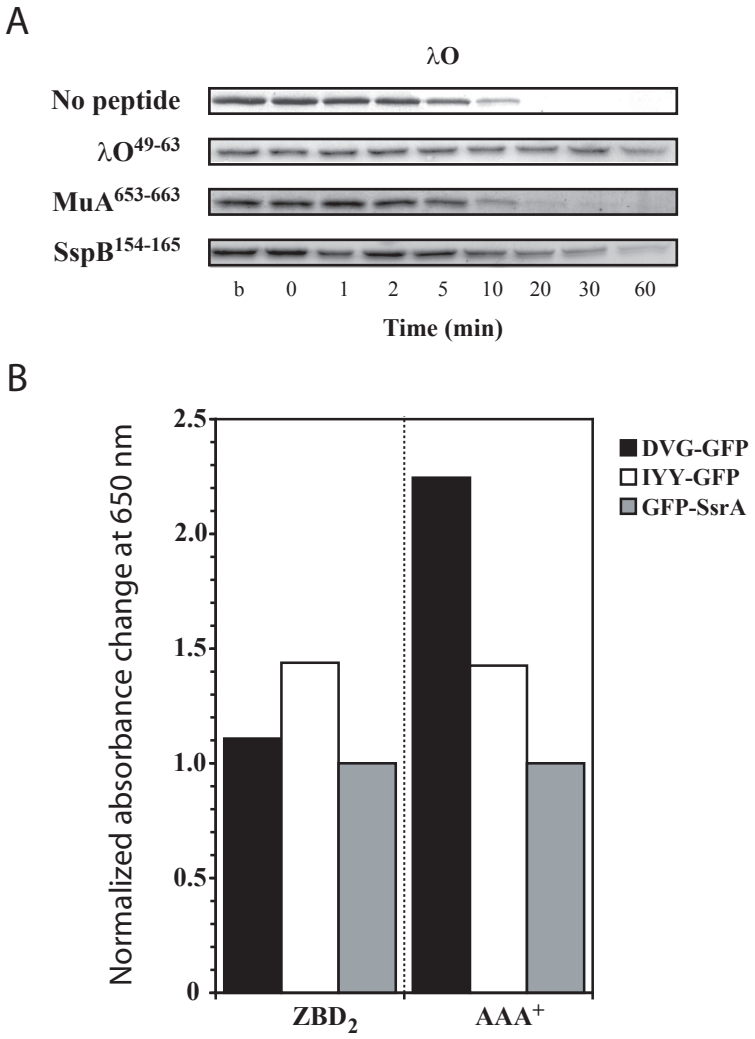

Supporting Figure 10

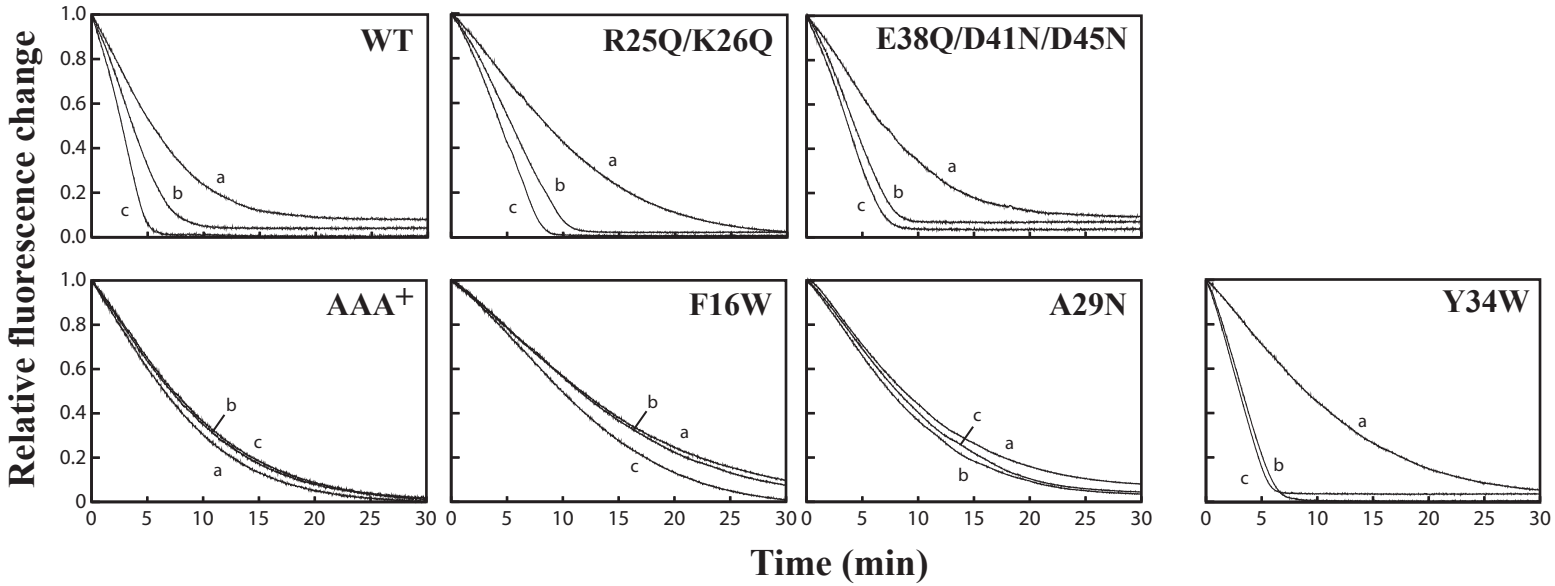

Supporting Figure 11

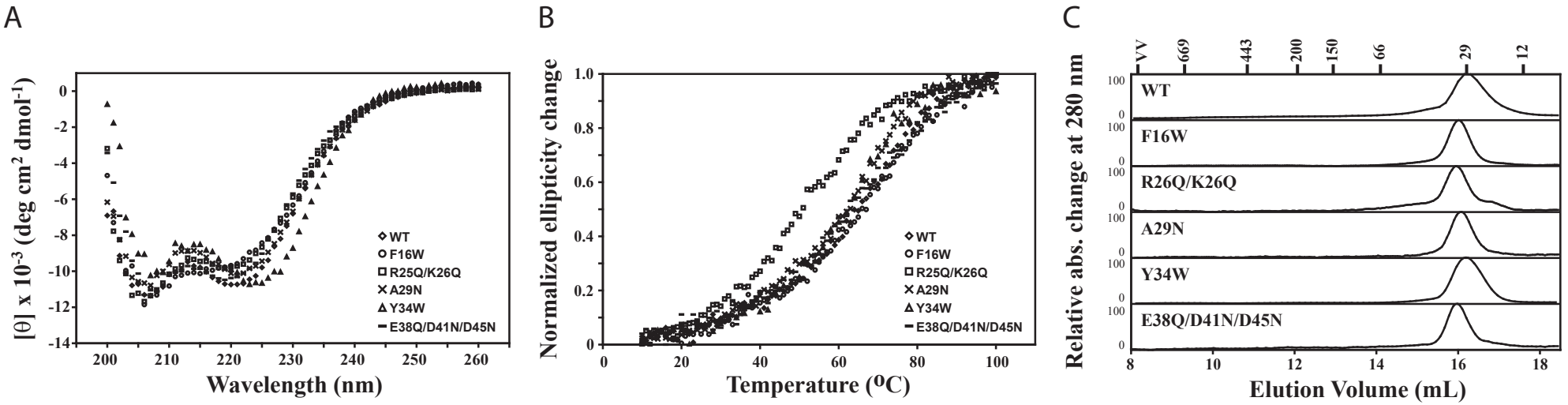

Supporting Figure 12

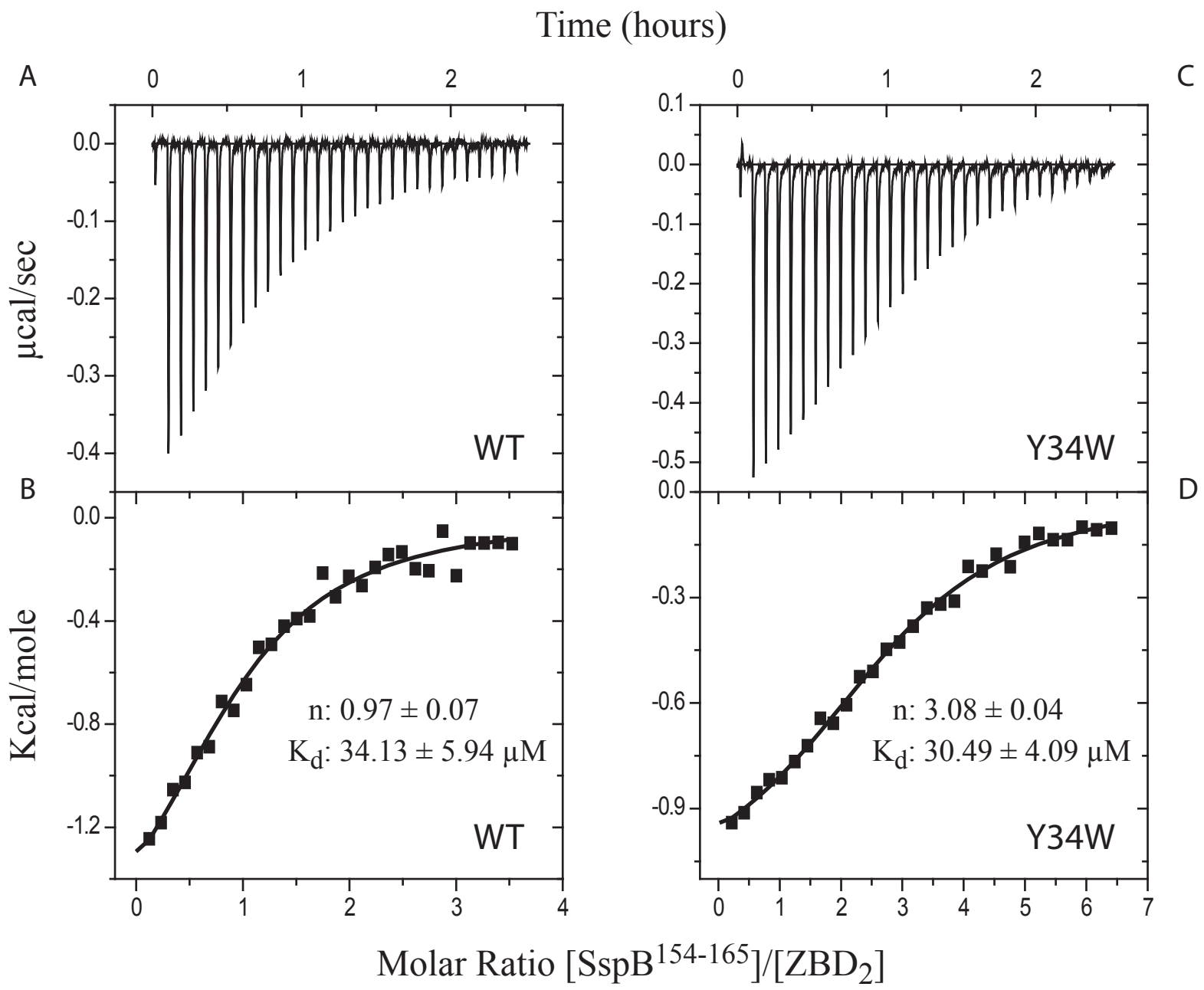

Supporting Figure 13

A

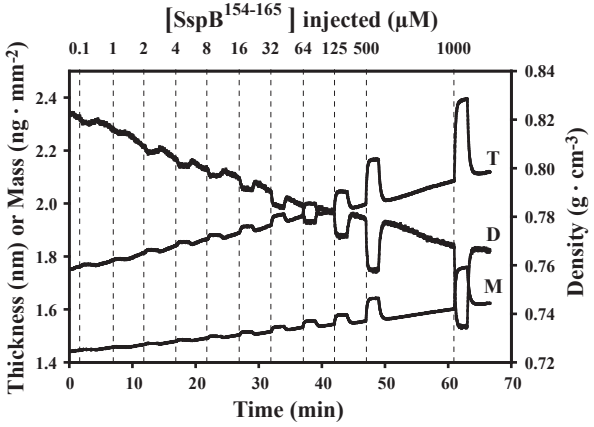

B

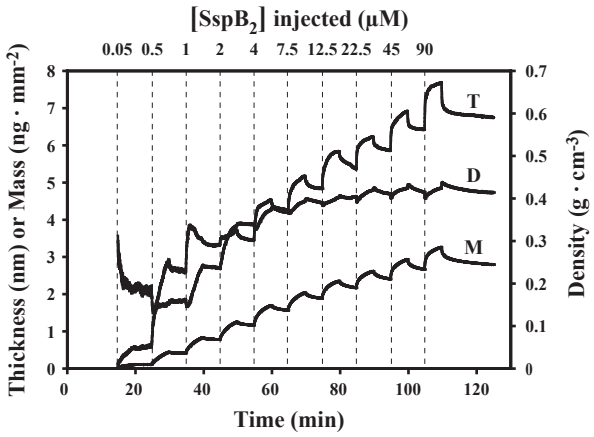

C

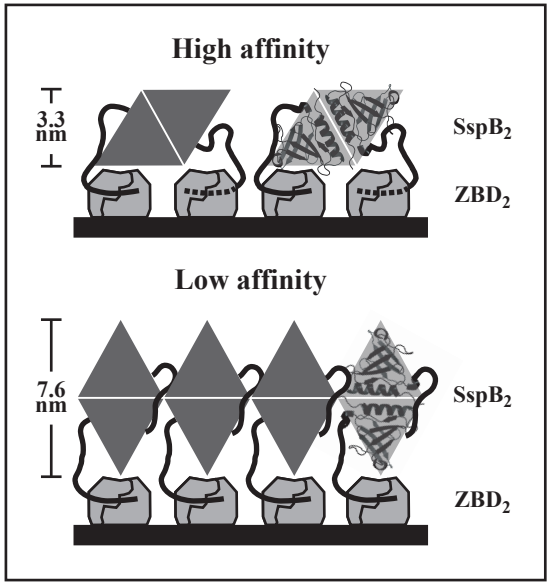

D

	ZBD_2	$SspB_2$ High affinity	$SspB_2$ Low affinity
Area ($Å^2$ $molecule^{-1}$)	1959	3768	1908